J. Fluid Mech. (2004), *vol.* 511, *pp.* 95–123.
DOI: 10.1017/S0022112004009528 Printed in the United Kingdom

Evolution of a turbulent jet subjected to volumetric heating

By AMIT AGRAWAL[1] AND AJAY K. PRASAD[2]

[1]Department of Mechanical Engineering, University of Newcastle, Callaghan, NSW 2308, Australia
Amit.Agrawal@newcastle.edu.au

[2]Department of Mechanical Engineering, University of Delaware, Newark, DE 19716, USA
prasad@me.udel.edu

(Received 3 February 2003 and in revised form 26 January 2004)

The goal of this study is to understand the effect of latent heat release on entrainment in cumulus clouds by employing a laboratory analogue consisting of a volumetrically heated turbulent axisymmetric jet. The jet fluid is volumetrically heated in an off-source manner to simulate condensation heat release in clouds. The experimental set-up is similar to Bhat & Narasimha (1996), and the current application of wholefield velocimetry and thermometry has allowed us to probe in detail the velocity and temperature fields within the heat injection zone (HIZ) for the first time, leading to several new results. We are able to demarcate three distinct zones within the HIZ based primarily on the nature of the cross-stream velocity profile, and we present sharp differences in flow properties in these zones. Thermochromic liquid crystal-based temperature visualizations have revealed details about the complex interplay of velocity, local concentration and temperature leading to a physically coherent understanding of this flow. We also provide evidence using linear stochastic estimates (LSE) to show that large eddies are disrupted in the latter part of the HIZ; the disruption of large eddies is linked to the change in the nature of the cross-stream velocity profile. While our results have confirmed certain previously reported observations such as a reduction in scalar width, we have measured significantly larger r.m.s. values within the HIZ than previously reported, which is corroborated by direct numerical simulation results.

We focus on the bulge in the scalar and velocity width at the start of the HIZ and link it to the excess deceleration of the centreline velocity there. Ideas proposed by Tso & Hussain (1989) are used to explain the eventual reduction of jet width with buoyancy addition. We also employ LSE to show that eddies are laterally compressed in ordinary jets, and that the surviving ones become more circular with heat addition in accordance with Lumley's (1971) hypothesis. Our primary conclusion differs from Bhat & Narasimha (1996) in that we measure a mass flux that exceeds that of an unheated jet throughout the HIZ. Further, we show that a step-increase in momentum flux corresponds to a step-increase in mass flux.

1. Introduction

Elavarasan *et al.* (1995, hereinafter referred to as EBNP) performed the first experiment using a laboratory analogue to measure the effect of latent heat release on entrainment in cumulus clouds. EBNP along with Bhat & Narasimha (1996) and Venkatakrishnan, Bhat & Narasimha (1999) (hereinafter referred to as BN and VBN,

FIGURE 1. Cumulus castellanus sprouting in tall towers in the Caribbean (with permission from Scorer 1972; photograph by Besty Woodward).

respectively) accumulated a substantial amount of data on the nature of the entrainment process in the presence of volumetric heating. The current paper is motivated by the same issues as these preceding works, and it is relevant to briefly recount them.

Cumulus clouds ascending through the atmosphere display a curious entrainment behaviour. Cumulus clouds are generally modelled as a plume which is driven upwards by buoyancy supplied at the source and entrains ambient fluid continuously through its lateral edges. The plume model works well until the cloud base is encountered, beyond which the continuously entraining model does not appear appropriate (Warner 1970). Although it is well known (Paluch 1979; Emanuel 1994) that cumulus clouds experience very little lateral entrainment, the reason for it is not evident.

Parcels of air ascend vertically in the atmosphere in the form of a plume or a thermal from a hot spot on the ground or the sea. These parcels experience adiabatic cooling due to expansion caused by a reduction in pressure with altitude. The parcel may contain water vapour, and cooling causes the ascending parcel to saturate with respect to water vapour at some level (the cloud base). Ascent beyond the cloud base results in condensation of excess water vapour into water droplets. Clouds are rendered visible beyond the cloud base by this condensed water vapour. The phase change of water is accompanied by latent heat release resulting in a temperature excess of 0.2–1 degrees in a typical cloud (Venkatakrishnan *et al.* 1998). As noted above, the laterally entraining plume model is applicable until the cloud base is encountered. Field observations (Paluch 1979) reveal that, beyond the cloud base, the lateral entrainment reduces to a negligible value, i.e. the added buoyancy from latent heat release significantly modifies the entrainment behaviour of the rising plume. Further, cumulus clouds are generally characterized by vertical boundaries, i.e. they exhibit almost no lateral spread (for an example, see figure 1, the photograph of cumulus castellanus clouds (from Scorer 1972)).

Clouds are, in general, complex flows because they contain multiple phases and can develop in a stably stratified atmosphere. The typical length and velocity scales in a cumulus cloud are 250–500 m and 2–4 m s^{-1}, respectively, resulting in a Richardson number of 0.1–2 (Venkatakrishnan *et al.* 1998). The thermodynamic aspects of a cloud have been explored in great detail; however, its fluid dynamical behaviour is

not as well understood (BN; VBN). One of the important fluid dynamical aspects is entrainment. Entrainment and mixing of the ambient air with the cloud affects important parameters such as the liquid–water content, ascent-height of the cloud, and precipitation. Therefore, the mechanism for the change in the mixing characteristics of the rising plume should be explored (BN). Moreover, the addition of an off-source body force to a free shear flow is of fundamental importance and its effect should be investigated (Hermanson & Dimotakis 1989; EBNP; Agrawal 2002).

Early attempts by Morton (1957), Squires & Turner (1962) and others to describe entrainment in cumulus clouds using a laterally entraining model, where air at a certain level comes solely from that level or below, failed to make realistic predictions in a cumulus cloud. Warner (1970) shows that the standard lateral entrainment model for plumes cannot simulatneously predict the height of ascent and air–water ratio in cumulus clouds. If the air–water ratio is matched, then the ascent height is underpredicted, while matching the ascent height of the cloud results in too little dilution. Heymsfield, Johnson & Dye (1978) found undiluted cloud base air at all levels within cumulus clouds. Paluch (1979) shows that the properties of air within cumulus clouds are attributable primarily to the mixing of air from below the cloud base with environmental air from near the cloud top, again attesting to the lack of lateral mixing. See Turner (1986) for a discussion on entrainment in geophysical flows, and Emanuel (1994) for a review of entrainment in cumulus clouds.

Our goal here is to apply whole-field measurement techniques to investigate this phenomenon of reduced lateral entrainment in cumulus clouds with the help of a laboratory heated water-jet experiment using the heating technique developed by Bhat, Narasimha & Arakeri (1989). We also compare these results with our concurrent direct numerial simulations (DNS). Of course, a laboratory experiment has length scales that are orders of magnitude smaller than the cloud, and the use of water as the working fluid precludes any possibility of replicating moist compressible convection in the atmosphere. Despite these shortcomings, the results indicate some qualitative features that are similar to cloud dynamics. Through the use of whole-field techniques for velocity and temperature, we have collected an extensive database that provides a deeper understanding of the volumetrically heated jet. Secondly, our detailed results should serve as a benchmark for modelling and computational efforts of buoyancy-added free shear flows.

Clouds are perhaps better modelled as plumes rather than jets. However, it is easier to construct a jet from an experimental viewpoint. Moreover, jets are somewhat better characterized than plumes in the literature. Therefore, we chose a laboratory analogue consisting of an axisymmetric turbulent jet for this work. We will now review previous work on cloud entrainment using laboratory analogues consisting of volumetrically heated jets and plumes. The purpose of this exercise is to review the current understanding of this flow, and to point out certain discrepancies in the current literature. We will also compare our results with the earlier findings in the later parts of the paper.

2. Previous studies

2.1. *Volumetrically heated jet*

The effort to simulate latent heat release in cumulus clouds using a laboratory analogue was pioneered by Narasimha's group at Bangalore. EBNP reported a disruption of coherent structures for the heated jet (Reynolds number, $Re = 1360$, Richardson number, $Ri \leqslant 0.2$) as compared to their unheated counterparts. EBNP reported that

the mass flux for the heated jet increases throughout the heat injection zone (HIZ), at a rate exceeding that of an unheated jet – the higher the heating rate, the greater is the increase. It is only in the post-HIZ that a drop in entrainment was observed.

BN showed that the divergence angle of the jet reduces with off-source heating, i.e. they found a reduction in the scalar width. They employed $1600 \leqslant Re \leqslant 3200$, while the analogous heating parameter (to be defined shortly) $G \leqslant 5$. Figure 10 of BN shows that all their mass-flux data-points within the HIZ lie well below the corresponding (at the same z/d) extrapolated values for the unheated jet, i.e. BN measured a drastic reduction in mass flux throughout the HIZ in comparison to an unheated jet. They attributed the disruption of coherent structures with volumetric heat addition as the reason for reduced entrainment.

Both BN and EBNP measured a decrease in the normalized streamwise velocity fluctuations with heat addition. However, they reported larger unnormalized fluctuations for the heated case as compared to the corresponding unheated counterparts. Therefore, BN believed that the disruption of large structures in a cumulus cloud leads to a virtually undiluted core (i.e. corresponding to regions near the centreline), while enhanced small-scale activity results in a higher rate of mixing in the outer regions of the flow.

2.2. *Volumetrically heated plume*

VBN conducted off-source volumetric heat addition experiments in plumes ($Re = 2500$, $Ri = 0.26$). They also found a reduction in spread rate with heat addition and disruption of large structures with heat addition. They found higher and slightly lower entrainment rates towards the beginning and end, respectively, of the HIZ. The relatively weak effect of heat on the mass flux of the plume was attributed to the low value of Ri employed in their experiment. They concluded that 'the much lower value of Ri in the present experiments while sufficient to cause a noticeable disruption of the eddy structure, is not enough to affect the mass flux appreciably.' VBN also measured a decrease in the normalized streamwise velocity fluctuations with heat addition, and a larger unnormalized fluctuation for the heated case as compared to the corresponding unheated counterparts. Furthermore, they found an enhanced activity of the smaller eddies.

Venkatakrishnan *et al.* (1998) investigated differences in heat addition on jets and plumes, and transition of jets to plumes in the post-HIZ. They found that plumes are more strongly affected than jets with heat addition, and a transition to plumes did not occur in the post-HIZ for their experimental conditions.

Narasimha, Saxena & Kailas (2002) applied wavelet analysis on instantaneous laser induced fluorscence (LIF) visualizations of heated plumes and showed that coherent structures are disrupted with heat addition. Further, they found that mixing activity was concentrated outside the core, and that the core itself was nearly homogeneous.

2.3. *DNS studies of volumetrically heated jets*

Basu & Narasimha (1999) performed DNS computations at $Re = 1600$ to investigate the effect of heat addition on jets, and the effect of different heating profiles on the jet. Their formulation consisted of a temporal analogue of the spatial problem. Basu & Narasimha (1999) found a reduction in the normalized fluctuations with heat addition. They found that a narrow heating profile affects the jet much more strongly, and found an increase in vorticity with heat addition for all cases investigated. They also found large expulsive motions at certain transverse cross-sections, and attributed this

as the reason for reduced entrainment in a heated jet. However, their computations employed periodic boundary conditions along the axial coordinate. Therefore, these computations could not conclusively provide evidence for a change in entrainment rate with heat injection.

Siddhartha *et al.* (2000) applied wavelet analysis to numerical data to investigate the effect of heat addition on the structures in a heated jet. They found that large structures telescope negligibly into their downstream counterparts for normal jets. However, the tendency to telescope increases with heat addition owing to the acceleration of the jet. Further, a complete breakdown of coherent motion was observed after prolonged heating.

2.4. *Modelling efforts*

Sreenivas & Prasad (2000) suggested that the positive centreline temperature gradient can impede the rate of overturning of the large eddies at the edge of a volumetrically heated jet. Large eddies are responsible for engulfing ambient fluid into the jet, and any effect that impedes their rate of overturning can adversely affect entrainment. They argue that within the HIZ, a downstream parcel of fluid on average is warmer than an upstream parcel owing to the former's higher residence time in the HIZ. Consequently, a stably stratified situation is obtained, and the large eddies experience a baroclinic torque which opposes the Biot-Savart induced torque. The net torque is weaker than the original Biot-Savart induced torque, and leads to a reduced overturning rate of the large engulfing eddies.

Govindarajan (2002) has constructed a simplified model based on vortex rings to help in the understanding of entrainment in volumetrically heated jets and cumulus clouds. She found that the tendency for a pair of vortex rings to leap-frog depends on the spacing between the two rings, and the relative velocity between the vortex ring and the external fluid. Govindarajan further demonstrated that entrainment can increase or decrease depending on the values of these parameters, and proposes this as the reason for reduced entrainment in a cumulus cloud, and an increased entrainment in a heated plume compared to a normal jet.

In summary, EBNP, BN and VBN using concentration (laser-induced fluorescence LIF) and point-wise laser Doppler velocimetry measurements, and BN, using DNS, examined the overall behaviour of the volumetrically heated jet or plume. They believed that the existing theories of entrainment are not sufficient to explain the reduced entrainment for this flow field (see BN), and discussed the implications of their study for entrainment in cumulus clouds. The knowledge developed from these previous studies has enabled us to now address several key and intriguing issues. We have significantly enhanced our understanding of this class of flows by conducting fresh experiments with the application of powerful diagnostic tools. Our purpose for undertaking this investigation is four-fold: (i) to apply whole-field velocimetry and thermometry to extract detailed flow and temperature data within the HIZ for the first time; (ii) to work in a larger parameter range; (iii) to elucidate the complex and simultaneous interplay of momentum, scalar concentration and buoyancy in three subzones within the HIZ and thereby obtain a physically coherent understanding of the flow; (iv) to evaluate the relevance of the existing entrainment theories to the present flow field. We will also compare our results for r.m.s. and mass flux with those obtained from DNS computations.

Data gathered from whole-field measurements within the HIZ have uncovered velocity and temperature features that have not been previously reported. While our results do confirm some previous findings, certain inconsistencies have come to the

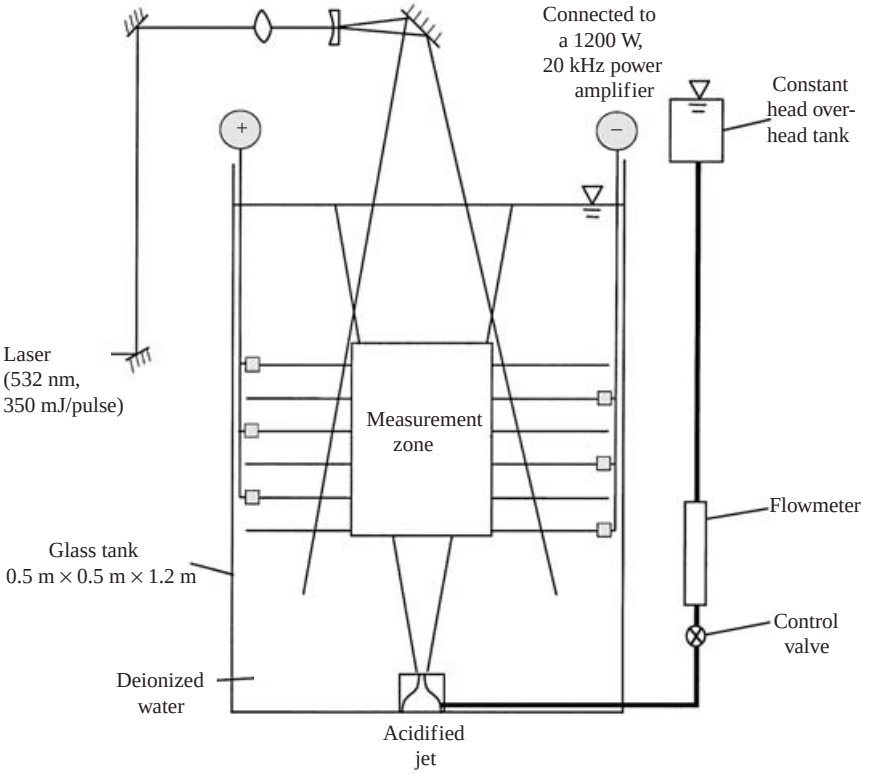

FIGURE 2. Experimental set-up.

fore. Our primary conclusion differs from BN: while BN believed that the mass flux reduces with heat injection, we conclude that heat addition leads to an increased mass flux.

3. Experimental set-up

Our experimental set-up is similar to that employed by EBNP and BN. Measurements were conducted in a 1.2 m tall glass tank with a 0.5 m square cross-section, which houses a nozzle (diameter $d = 2$ mm) at the bottom. The jet was directed upwards, as shown in figure 2. The jet water was made electrically conducting by adding a small amount (≈ 15 ml l^{-1}) of hydrochloric acid to it while the ambient fluid was deionized water and was therefore electrically non-conducting (Bhat *et al.* 1989). The heat injection zone (HIZ) consisted of six wire grids (wire diameter 150 μm) spaced 2.5 cm apart along the axial direction. Selective ohmic heating of the jet fluid occurs owing to its highly elevated electrical conductivity thereby raising the jet fluid temperature over that of the ambient fluid.

The axial plane of the jet was illuminated by a 1 mm thick light sheet from twin Nd:YAG pulsed lasers (350 mJ/pulse at 532 nm). Images were recorded at 0.5 Hz using a Kodak 1.0 ES CCD camera with a 1026×1000 pixels array. Fluorescent particles of size 20–40 μm were used as tracers for particle image velocimetry (PIV) and the pulse separation for PIV measurements was 36 ms. A long-wave filter was placed in front of the camera lens to block elastic scattering (at 532 nm) from the grids while passing the fluorescent scattering from the particles. Note that the upwardly

pointing turbulent axisymmetric jet simulates the ascending cloud, while the off-source volumetric heat addition simulates the latent heat release effect in cumulus clouds.

Rhodamine 6G was used for LIF, and temperature measurements were accomplished using 40 μm micro-encapsulated thermochromic liquid crystals (TLC) which serve as temperature sensors. The wavelength of light that is preferentially scattered by the TLC depends on its temperature. Owing to its small size, the response time of the micro-encapsulated TLC is a few milliseconds, implying that the temperature of the TLC corresponds closely to the fluid that carries it. See Agrawal, Sreenivas & Prasad (2004*b*) and Agrawal & Prasad (2002*a*) for additional details of the experimental setup.

To quantify the effect of heat, the non-dimensional heating number, Ri or G (BN) and Re are used.

$$G = \frac{\alpha g}{\rho C_p}\frac{z_b^2}{d^3}\frac{Q}{U_0^3}, \quad Re = \frac{U_0 d}{\nu}, \tag{1}$$

where α is the coefficient of thermal expansion, g is the acceleration due to gravity, ρ is the density of the unheated fluid, C_p is the specific heat, z_b is the axial distance from the nozzle where heating starts, Q is the total power (watts) added to the jet, U_0 is the nozzle exit velocity and ν is the kinematic viscosity. The Richardson number employed by EBNP is equivalent to G expressed in local rather than nozzle scales, i.e. with d and U_0 replaced by b and U_c, respectively, where b is the local jet width and U_c is the local centreline velocity. In fact, $G = 12.5\,Ri$ (Agrawal *et al.* 2004*b*). The term b is defined as the radial location where the mean streamwise velocity is e^{-1} of the mean centreline velocity U_c.

The range of G (or Ri) for the present investigations is much larger and enables us to observe features which have not been previously reported. Although most of the results are presented for $G = 4.3$, the same qualitative trends can be discerned at higher values of G.

4. Unheated (normal) jet

A set of baseline experiments was carried out to characterize the normal (unheated) jet flow (see Agrawal *et al.* 2004*b* for relevant plots) and to check whether the flow was affected by the presence of the grids. Both LIF and PIV results (including second-order moments) were virtually identical with and without grids, confirming that the grids did not affect the flow. We confirmed that the streamwise velocity profile at each downstream location is approximately Gaussian in nature. The cross-stream velocity profiles are also in good agreement with theory (Agrawal 2002). Specifically, the cross-stream velocity profile is positive in the vicinity of the centreline, and experiences a zero-crossing at $r/b \approx 1.1$, i.e. the jet experiences an outflow $r/b < 1.1$ and an inflow for larger r/b (r is the radial coordinate).

Figure 3 shows the radial variation of the normalized r.m.s. for the streamwise and cross-stream velocity components. The mean normalized r.m.s. value at the centreline is 0.26 for the streamwise component, and 0.19 for the cross-stream component in excellent agreement with previous results (e.g. Hussein, Capp & George 1994; Boersma, Brethouwer & Nieuwstadt 1998).

5. Volumetrically heated jet

5.1. *Variation in instantaneous and mean fields*

Substantial LIF image analysis of volumetrically heated jets has already been presented in the literature (EBNP; BN). We therefore do not elaborate on scalar

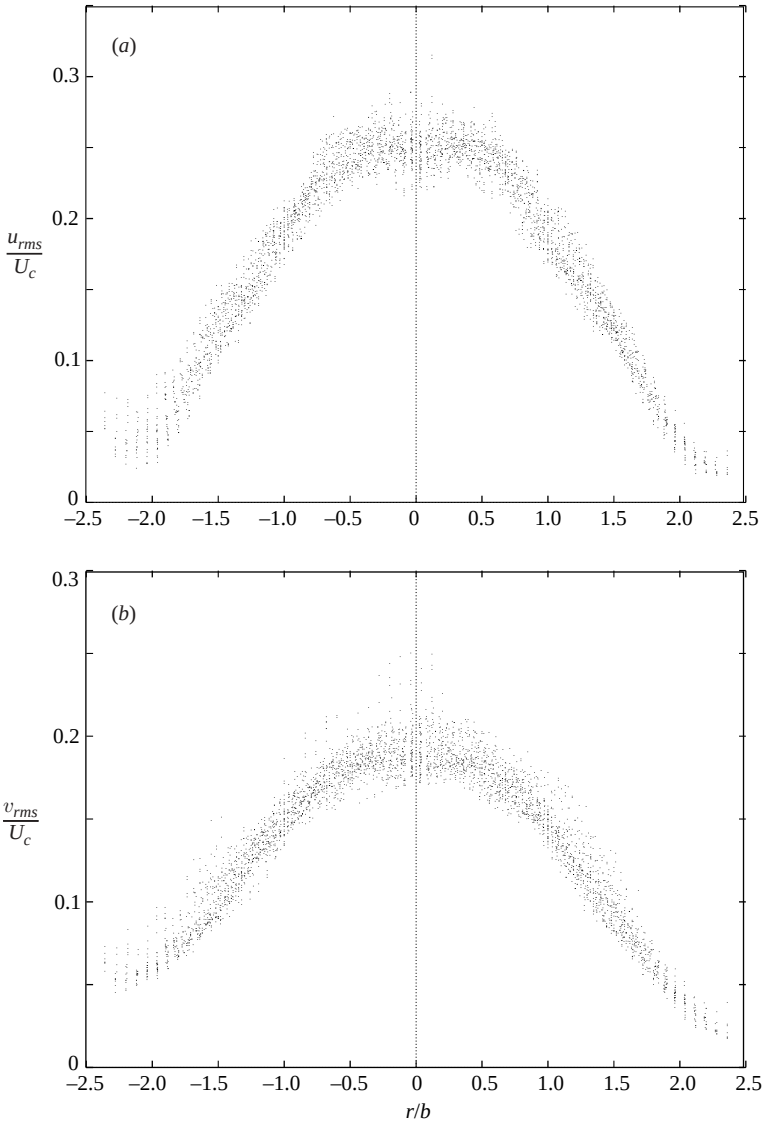

FIGURE 3. Normalized fluctuations of the (*a*) streamwise and (*b*) cross-stream velocities ($Re = 3000, 110 \leqslant z/d \leqslant 175$).

measurements here, other than to provide a visual confirmation of disruption of large eddies and reduction in scalar width heat addition. An example of an instantaneous LIF image is given in figure 4 ($155 \leqslant z/d \leqslant 255$, $Re = 2000$, $G = 9.2$) where both these features are clearly evident (z is the axial coordinate). A direct comparison of instantaneous and time-averaged heated and unheated jets can be found in Agrawal *et al.* (2004*b*).

Figure 5 is an example of a TLC image ($Re = 1450, 202 \leqslant z/d \leqslant 267, G = 13.5$). More information can be gleaned from TLC frames as compared to LIF, because unlike the dye, these crystals are present both in the jet and the ambient fluid. The differences in colour further provide an indication of the amount of mixing of the ambient and jet fluids. The ambient in figure 5 is at 23.5 °C (red), while the jet fluid

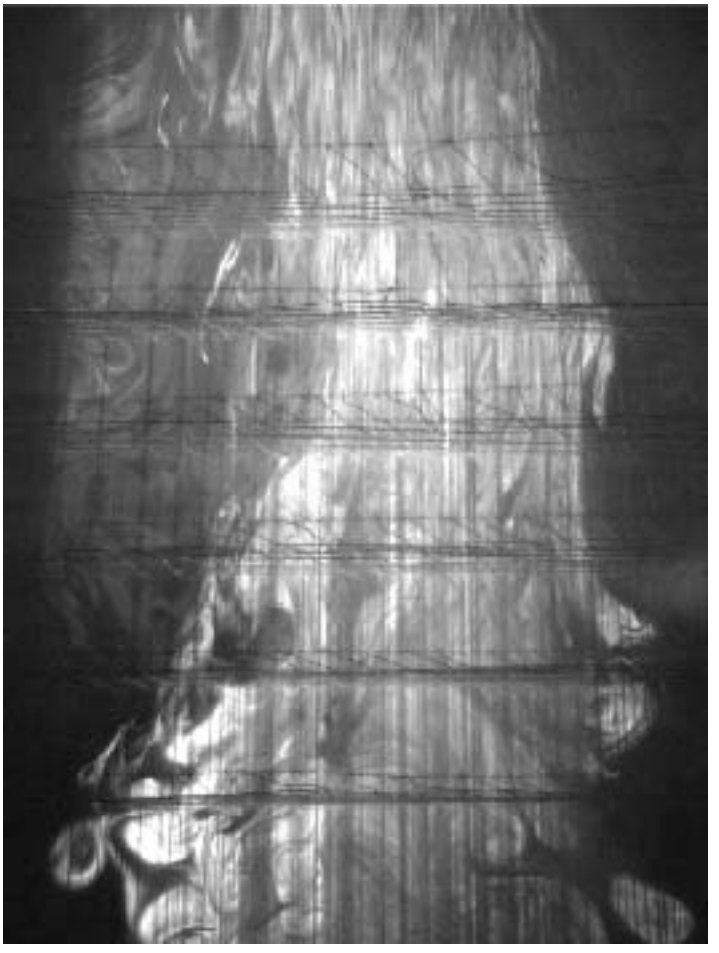

FIGURE 4. LIF visualization for $155 \leqslant z/d \leqslant 255$ ($Re = 2000$, $G = 9.2$). The flow is from bottom to top. Bright horizontal lines in the viewframe indicate location of the grids, while dark vertical lines are shadows from the wires.

changes from the ambient colour near the bottom of the frame to blue near the top. This indicates that, initially, the jet is at the ambient temperature (as expected), and the temperature increases with the axial coordinate due to heat addition. The sharp demarcation of colours at the jet boundary, along with almost no change in colour of the ambient fluid, indicates that the jet fluid is indeed being selectively heated. Blue (hot) streaks can also be seen originating at the wire grids in the TLC frame. This is due to convergence of electrical paths at the wires which results in a slightly larger heating in the vicinity of the wires. Therefore, heating is not perfectly uniform inside the HIZ. However, no noticeable effect of this non-uniformity was detected in our results. The slight non-uniformity in heat injection is a limitation of this volumetric heating technique.

We can make three important observations by comparing the jet before the second grid (in the frame) with the jet downstream of this grid location. First, the narrowing of the jet is apparent beyond the second grid; secondly, large eddies are observed upto this axial location and are less apparent beyond it; thirdly, the jet appears to be axially stretched beyond the second grid. The disruption of large eddies might

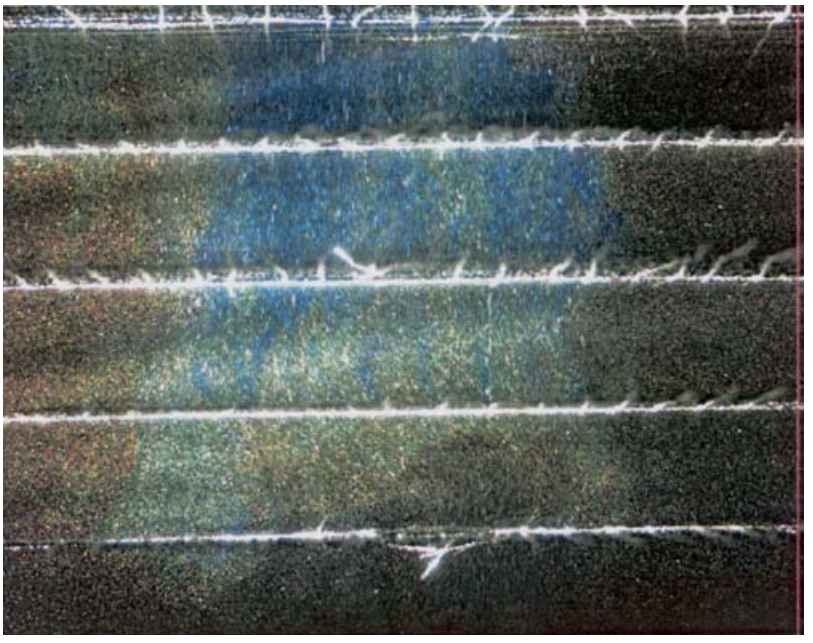

FIGURE 5. Temperature visualization in a heated jet (red = cold, blue = hot) ($Re = 1450$, $G = 13.5$) (Agrawal *et al.* 2004*b*). The flow is from bottom to top.

partly be the reason for the observed decrease in the spread rate as discussed in § 7.1. Figure 5 also indicates that for an axial location upstream of the fourth grid, the temperature increases with r and then decreases, implying that the maximum temperature is located away from the centreline. This observation is confirmed by time-averaging the individual temperature fields between the third and fourth grids (Agrawal *et al.* 2004*b*). They explained this off-axis maximum temperature as being due to the competing effects of local acid concentration and residence time.

The HIZ is in the range $200 \leqslant z/d \leqslant 265$ for PIV measurements while the viewframe is in the range $200 \leqslant z/d \leqslant 289$ encompassing the region affected most severely by heat injection. Therefore, similar to BN and cumulus clouds, the extent of the HIZ is two to three times the nominal jet width. We have 337 statistically independent results obtained from three runs providing almost equal numbers of realizations. The scatter within the runs was verified to be within experimental error. The jitter in the profiles is due to the presence of the grids and not because of inadequate averaging. The results in this subsection have been discused more extensively in Agrawal *et al.* (2004*b*).

We found that the cross-stream velocity profile can be used to demarcate the viewfield into three zones. The lower zone (zone 1) results reveal that the shapes of the velocity profiles are as yet unaltered by heat addition – the streamwise velocity is still Gaussian in nature (figure 6) and the cross-stream velocity profile exhibits an outflow for small r and shows a tendency to turn inwards at larger r (figure 7). These profiles closely resemble the baseline jet. In the middle zone (zone 2) the cross-stream velocity is nearly zero for all r in the viewing zone (figure 7), i.e. the region of mass outflow is not observed close to the jet centreline. The streamwise velocity in zone 2 is in a transitional state between zones 1 and 3 (figure 6). The upper zone (zone 3) shows a strong effect of heating on the jet: the streamwise velocity profile changes

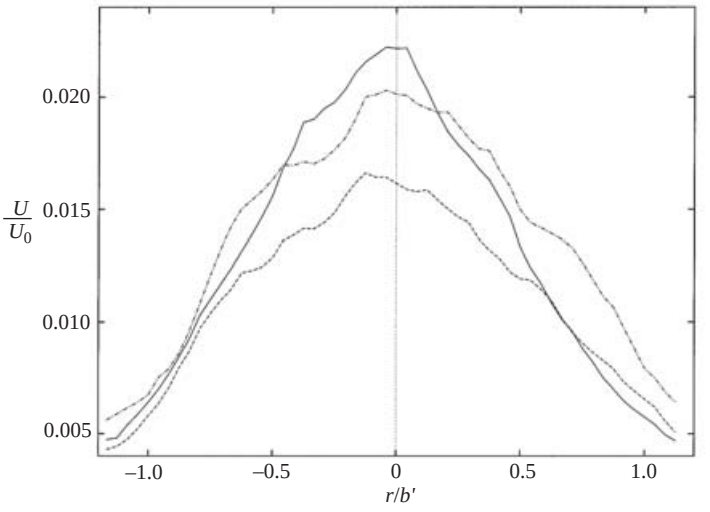

FIGURE 6. Streamwise velocity profiles for different zones: —, zone 1; – – –, zone 2; – . –, zone 3. ($Re = 2400$, $G = 4.3$, b' is the nominal jet width corresponding to the mid-z location of the viewframe) (Agrawal *et al.* 2004*b*).

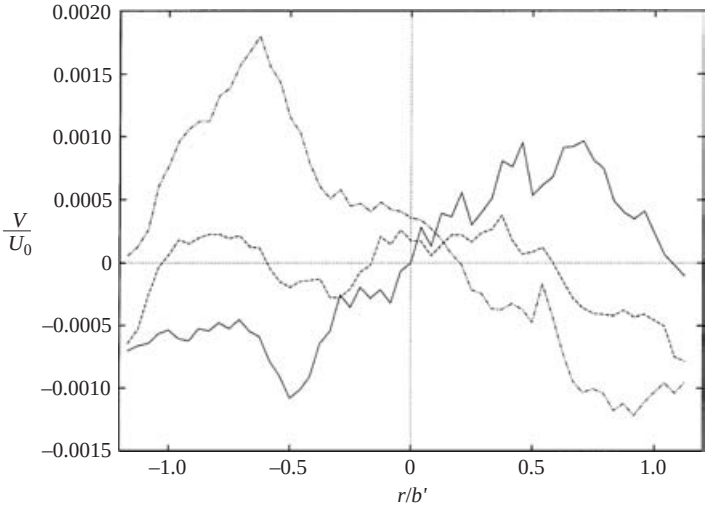

FIGURE 7. Cross-stream velocity profiles for different zones ($Re = 2400$, $G = 4.3$) (Agrawal *et al.* 2004*b*). Key as in figure 6.

from a Gaussian to a flat-top Gaussian profile (figure 6). The cross-stream velocity V (figure 7) is inward for small r and tends to 0 farther out, i.e. a mass inflow is seen for all r in this zone. This indicates that the mass flux should increase in zone 3 relative to the unheated jet.

Figures 6 and 7 together lead to the conclusion that as the jet enters the HIZ, its streamwise and cross-stream velocity profiles are not significantly affected in shape because the jet is still decelerating here (figure 8). As the jet progresses into zone 2,

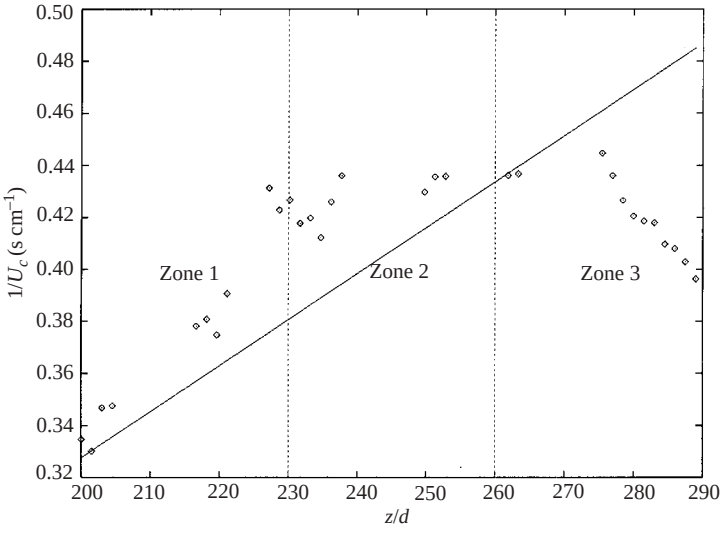

FIGURE 8. Centreline velocity for —, normal and ◇, heated jets ($Re = 2400$, $G = 4.3$) (Agrawal *et al.* 2004b).

the profiles change in response to an arrest in the decay of the centreline velocity (figure 8). The jet eventually begins to accelerate owing to the cumulative effect of heat addition in zone 3 and the cross-stream velocity responds by indicating a mass influx at all radial locations, and the streamwise velocity responds by becoming flatter at the centreline, allowing a larger streamwise momentum flux. Previous studies have not discerned these features in the mean velocity profiles within the HIZ. For example, BN provide radial profiles of the streamwise velocity only for the post-HIZ. Even here, the changes in the velocity profiles could not be resolved, probably because of the sparseness of data points in the radial direction. Furthermore, the cross-stream velocity, which is the key indicator for the different zones has not been previously measured. Figure 8 reveals an excess deceleration of streamwise velocity at the beginning of the HIZ. A larger relative deceleration at the beginning of the HIZ can also be seen in the data of VBN for volumetrically heated plumes. Although BN did not report this excess deceleration, they observed a small acceleration of the jet at the end of the HIZ and the beginning of the post-HIZ. See Agrawal *et al.* (2004*b*) for an interesting discussion on the coupling between the cross-stream velocity and the variation of the centreline velocity.

The velocity width (figure 9) of the jet increases rapidly in the initial part of the HIZ, and then remains almost constant. The initial increase in the velocity width is large enough to ensure that the velocity width throughout the HIZ exceeds that of a normal unheated jet. BN also allude to this result, albeit on the basis of only three data points (within, at the end, and beyond the HIZ). The increase in velocity width over-and-above that for a normal jet during the initial part of the HIZ is expected because momentum which varies as $b^2U_c^2$ must increase with z owing to heat addition, whereas U_c is seen to decrease faster than z^{-1} (figure 8). We will provide another reason for this observation in § 5.4. The subsequent plateauing of velocity width might be linked to a decrease in the scalar distribution width. Therefore, this result is in contrast with the scalar width (see figure 6 of BN) which becomes smaller than for

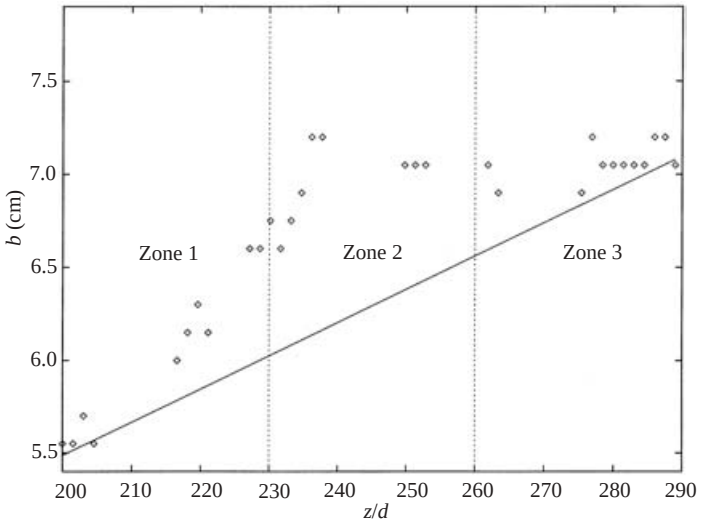

FIGURE 9. Velocity widths for —, normal and ◇, heated jets ($Re = 2400$, $G = 4.3$) (Agrawal *et al.* 2004*b*).

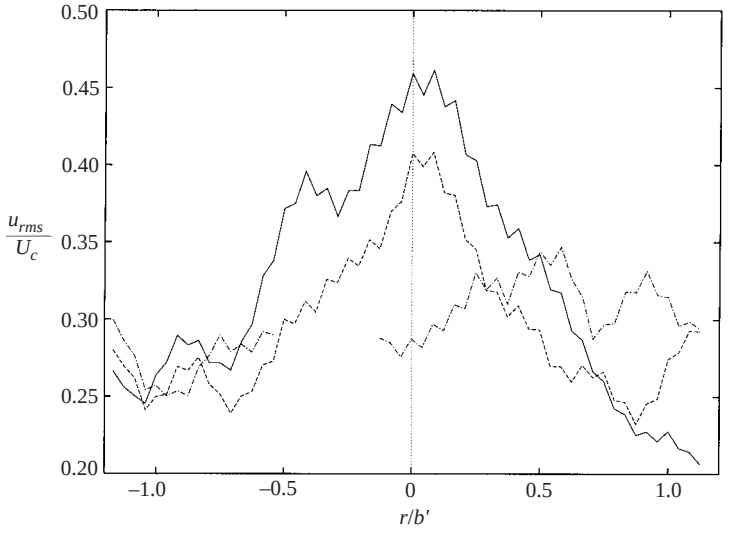

FIGURE 10. Normalized fluctuations of the streamwise velocity in the three zones. Key as in figure 6. $Re = 2400$, $G = 4.3$, b' is the nominal jet width corresponding to the mid-z location of the viewframe. (Zone 3 data for $-0.5 < r/b' < -0.2$ was corrupted by strong localized reflections from the wire grids and are omitted).

a corresponding unheated jet in the latter part of the HIZ. VBN have presented the velocity width for plumes.

5.2. *Variation in r.m.s. values*

Figure 10 shows the radial variation of the normalized r.m.s. for the streamwise component of velocity (r.m.s. divided by the mean streamwise velocity at the jet

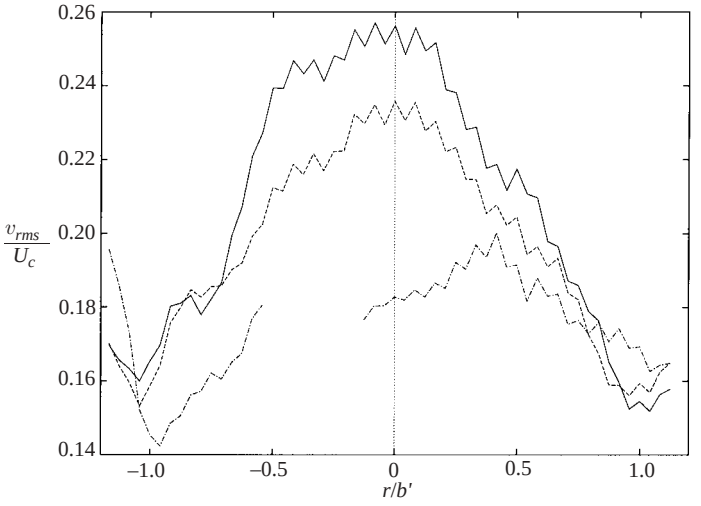

FIGURE 11. Normalized fluctuations of the cross-stream velocity in the three zones ($Re = 2400$, $G = 4.3$). Key as in figure 6.

centreline). It can be seen that $\sqrt{\langle u'^2 \rangle}/U_c$ is substantially larger (by about 60%) than in a normal jet in zone 1. Probable reasons for this increase are discussed later in the section. The centreline value reduces somewhat in zones 2 and 3, but still remains larger than in normal jets. An increase in the normalized streamwise fluctuations with heat addition indicates that although the jet fluid is being axially stretched, relaminarization of the jet does not occur. The profiles for normalized r.m.s. in zones 1 and 2 are similar to a normal jet, i.e. maximum at the jet centreline and decreasing monotonically with increasing radial coordinate. However, the r.m.s. profile in zone 3 undergoes a change in shape: the normalized value is nearly constant at 0.29 for the radial extent shown in figure 10, and is expected to diminish for larger r.

Similar to $\sqrt{\langle u'^2 \rangle}/U_c$ the magnitude of $\sqrt{\langle v'^2 \rangle}/U_c$ at the centreline decreases as we traverse from zones 1 to 3. The magnitude of $\sqrt{\langle v'^2 \rangle}/U_c$ for heated jets is larger than unheated jets in zone 1, and becomes almost the same in zone 3. The shapes of the profiles in zones 1 and 2 are similar to normal jets (figure 11), however, the shape of the cross-stream r.m.s. profile appears to change in zone 3. The normalized value is nearly constant at 0.18 for a small radial extent about the centreline, and reduces monotonically for larger radial positions.

The mean streamwise velocity profile is a flat-top Gaussian for zone 3, and figures 10 and 11 indicate that the normalized r.m.s. value is also nearly constant near the jet centreline. It therefore appears that heat injection causes both the mean as well as the normalized fluctuations of velocities to assume uniform values near the jet centreline.

The axial variation of normalized r.m.s. for the streamwise and cross-stream components of velocity at the centreline is summarized in figure 12. Note that figures 10 and 11 represent average values for each subzone, whereas actual values at the centreline are plotted in figure 12, resulting in a slight mismatch in the values. Both r.m.s. quantities decrease monotonically with the axial coordinate. The large difference in normalized r.m.s. between the unheated and heated jets warrants some explanation. The axial variation in U_c can partly explain the observed behaviour of the normalized fluctuations. For example, a large increase in $\sqrt{\langle u'^2 \rangle}/U_c$ in zone 1 is partly due to the reduction in U_c in zone 1 (figure 8). Similarly, the subsequent

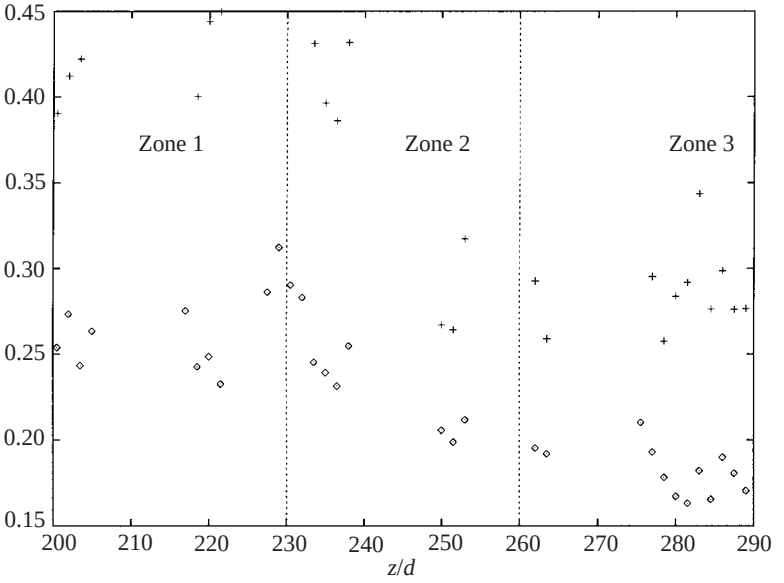

FIGURE 12. Axial variation of the normalized +, streamwise and ◇, cross-stream fluctuations.

drop in the normalized r.m.s. values is partly due to an increase in U_c in zones 2 and 3. Similarly, we can argue that due to the axial variation of U_c, $\sqrt{\langle v'^2 \rangle}/U_c$ will increase in zone 1, and will subsequently decrease. However, even after adjusting for the change in U_c in various zones, the difference in $\sqrt{\langle u'^2 \rangle}/U_c$ between unheated and heated jets remains substantial, indicating that additional mechanisms are operational here.

We propose two mechanisms that can increase the unnormalized fluctuations. First, a substantial presence of small intense eddies created by heat addition could generate this large increase in the streamwise fluctuations. Such smaller eddies have been seen, for example, in the computations of Basu & Narasimha (1999). Secondly, as the jet enters the HIZ, the jet fluid becomes selectively heated and starts to accelerate; however, the upstream jet fluid is still slow-moving. A point in the HIZ may therefore intermittently experience parcels of fluid that move faster or slower than the mean, resulting in a large value of r.m.s. for the streamwise velocity. This mechanism was identified while carefully following the heated jet in the DNS studies of Agrawal, Boersma & Prasad (2004*a*). Further, it appears that this effect of acceleration is maximum towards the beginning of the HIZ, resulting in a maximum $\sqrt{\langle u'^2 \rangle}/U_c$ in zone 1 and a subsequent reduction beyond it (figure 12). However, these effects are expected to result in a smooth increase in r.m.s. and therefore a sudden increase at the beginning of the HIZ is unexpected.

We initially suspected that the presence of heating grids might contribute to this increased r.m.s. However, r.m.s. measurements in the absence of heating, but with grids present, yielded r.m.s. values that closely matched the values quoted in the literature for ordinary jets (§4). Therefore, we believe that heat injection indeed increases the normalized r.m.s. We turned to our concurrent DNS of heated jets (see Agrawal *et al.* 2004*a* and §6) for additional confirmation, which suggest that r.m.s. can indeed increase sharply, albeit within the HIZ with heat addition, and the maximum normalized r.m.s. value of 0.45 in our DNS study agrees very well with the present experiments. We will show in §5.4 that a step change in momentum flux correlates

with a step increase in mass flux. It is conjectured that there is a corresponding step change in r.m.s. as well. It is also possible that upstream effects which occur beyond our viewfield can produce this sudden increase in streamwise r.m.s. Better resolved measurements are clearly needed at the base of the HIZ to clarify this issue. It is noteworthy that figure 5 of VBN indicates a similar trend.

It should be noted that previous workers (EBNP; BN) have reported a decrease in the normalized value of streamwise fluctuations. However, similarly to the present study, VBN (see their figure 5) found a larger normalized r.m.s. as compared to the baseline case at the beginning of the HIZ, and a subsequent reduction in its value. The difference in the normalized r.m.s. between the present study and those of EBNP and BN is substantial. In an attempt to understand the differences between present and previous studies, we examine the magnitude of the unnormalized fluctuations from the relevant sources. This quantity is normally not reported and has to be deduced from the normalized r.m.s. and centreline velocity. Basu & Narasimha (1999, figure 5*c*) reported a maximum increase of about 100% in the unnormalized streamwise fluctuation for their largest heat injection rate. However, their corresponding centreline velocity increased by 240%, resulting in a 40% decrease in the normalized r.m.s. (see their figures 5*b* and 5*d*). From figures 9(*a*) and 9(*b*) of BN, the magnitude of the unnormalized fluctuation in the middle of the HIZ can be deduced as follows: for their largest heating parameter of $G = 4.2$ and $z/d = 173$, the normalized fluctuations decrease by about 25%, while the centreline velocity increases by $\approx 15\%$. This implies that the unnormalized fluctuation should decrease by about 10%. Similar calculations for other locations within and just beyond the HIZ reveal that the unnormalized fluctuation of streamwise velocity of BN either decreases slightly or does not change significantly when compared to the unheated jet.

Our results indicate a maximum decrease in the centreline velocity of about 15% which corresponds to a maximum increase of 60% in the normalized r.m.s. This indicates that the maximum increase in the unnormalized fluctuations can reach 45%, which is well within the range obtained by Basu & Narasimha (1999). An increase in the unnormalized fluctuations is expected because of the two additional mechanisms identified earlier, and is consistent with the computations of Basu & Narasimha. On the other hand, it is not apparent why such large differences in the normalized r.m.s. should arise between the different studies.

The shapes of the normalized Reynolds stress profiles for the three zones were found to be similar to the corresponding unheated jet – zero at the jet centreline, maximum for $r/b \approx 0.6$, and a monotonic decrease for larger r/b (Agrawal 2002). However, the peak normalized Reynolds stress appears to decrease somewhat from zones 1 to 3.

5.3. *Disruption of large eddies*

EBNP, BN, VBN, Venkatakrishnan *et al.* (1998), Siddhartha *et al.* (2000) and Narasimha *et al.* (2002) have reported a disruption of large engulfing eddies in turbulent jets and plumes with heat injection. This deduction was based on LIF visualizations and analysis of DNS data. Here, we will first present an LIF result and then apply the technique of linear stochastic estimation to PIV data to show that the large eddies are disrupted in the latter part of the HIZ.

Stochastic estimation is a useful tool to reconstruct a velocity field conditioned upon one or more events, from a set of whole-field velocity data (Adrian 1994;

Gieseke & Guezennec 1994), and is somewhat equivalent to conditional averaging of point-wise data. A large data-set of instantaneous PIV vector fields collected under identical conditions, and one (or more) event vector(s) are the inputs to this technique. The output (estimated field) is obtained by minimizing the root-mean-square error between the estimated and the instantaneous input fields. It should be noted that owing to its least-squares nature, a stochastic estimate need not resemble any of the instantaneous data-fields that serve as the input. The technique has been successfully employed to educe both the underlying and the dominant structures in stationary turbulent flows (e.g. Prasad & Gonuguntla 1996; Agrawal & Prasad 2002*b*).

The LIF visualization of figure 4 and the temperature visualization of figure 5 indicate an axial stretching and narrowing of the jet beyond the first grid. Further, eddies are visible upstream of this grid, but are not apparent downstream of it, indicating that although heat is added throughout the HIZ, its disruptive effect on coherent structures is felt only in the latter part of the HIZ. Previous studies fail to recognize that the disruption of eddies occurs only in the latter part of the HIZ. Furthermore, the location beyond which disruption of eddies occurs moves upstream with an increase in the amount of heat addition.

Figure 13 shows a two-point stochastic estimate for the unheated and heated jets. Note that the PIV data is Galilean transformed and low-pass filtered prior to stochastic estimate calculations (see Agrawal & Prasad 2002*b* for details). Events (1, 0) at (15, 2) and (−0.4, 0) at (48, 23) are specified in both the cases. Here, each event vector represents the user-specified cross-stream and streamwise velocity components. The specified events lead to the emergence of a helical mode with vortices centred at (12, 13), (52, 33) and (9, 53) for the unheated jet (figure 13*a*). Presence of such modes has been reported previously (e.g. Tso & Hussain 1989; Siddhartha *et al.* 2000). Vortices centred at (12, 13) and (9, 53) are located on the left of the time-averaged jet axis and rotate counterclockwise, while the vortex at (52, 33) rotates clockwise, as expected of large vortices. (However, small vortices on both sides of the jet axis may rotate in either direction, Agrawal & Prasad 2002*a*.) In contrast, the specified events spawned only one vortex centred at (10, 11) (and therefore in zone 1) in the heated jet rotating counterclockwise (figure 13*b*) with a size similar to the educed vortex at (12, 13) in figure 13(*a*). Incomplete and indistinct vortices (figure 13*b*) occupy locations corresponding to the two downstream vortices in the unheated jet (figure 13*a*). The clearly weaker signatures of the downstream vortices indicate that heat injection disrupts large eddies in the latter part of the HIZ. On a cautionary note, the axial locations and magnifications are different for the two frames (as indicated in their captions). Therefore, figures 13(*a*) and 13(*b*) must be compared with care.

The disruptive effect of heat injection on eddies can now be explicitly linked to the changing nature of the mean radial profile of cross-stream velocity in the latter half of the HIZ. In an unheated jet, the radial region of outflow extends to $r/b = 1.1$. Therefore, while traversing a path parallel to the jet axis, we expect to see both inward and outward velocities in the neighbourhood of the intersection of this path with the jet edge (i.e. at $r \approx b$). The mean cross-stream velocity is inward upstream of the intersection point, and outward downstream of it. The opposing directions of cross-stream velocity surrounding the intersection point provide the necessary condition required to close the streamlines for a vortex. In contrast, for heated jets, the cross-stream velocity profile in zones 2 and 3 indicates an absence of outflow in the vicinity of the jet axis (figure 7). The absence of a mean outflow region suppresses the outward pointing vectors on the downstream side of large vortices. Consequently, the streamlines do not appear closed for the heated jet, and suggest that large vortices

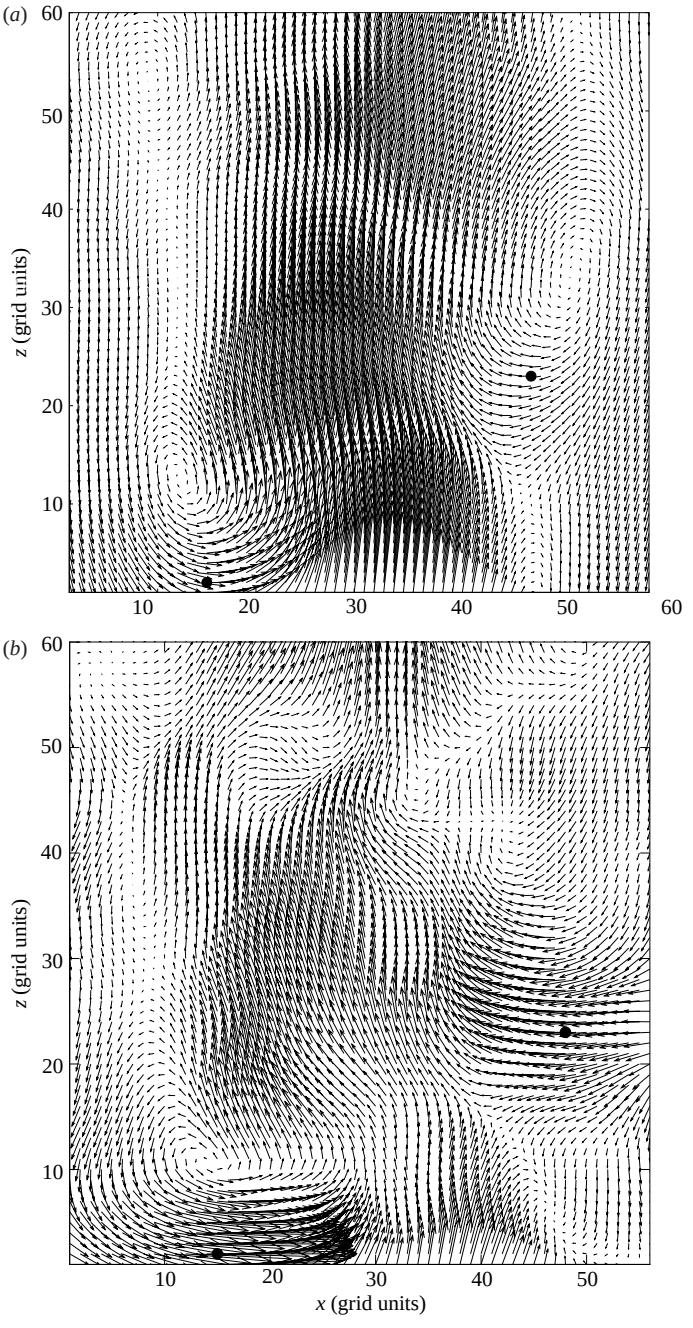

FIGURE 13. Two-point stochastic estimate for (a) unheated jets ($110 \leqslant z/d \leqslant 175$, 1 grid unit = 2 mm) and (b) heated jets ($200 \leqslant z/d \leqslant 289$, 1 grid unit = 3 mm). The black dots indicate locations of the specified events.

are weakened or disrupted. These observations are consistent with the role of stable stratification in suppressing the formation of large eddies within the heated jet as proposed by Sreenivas & Prasad (2000).

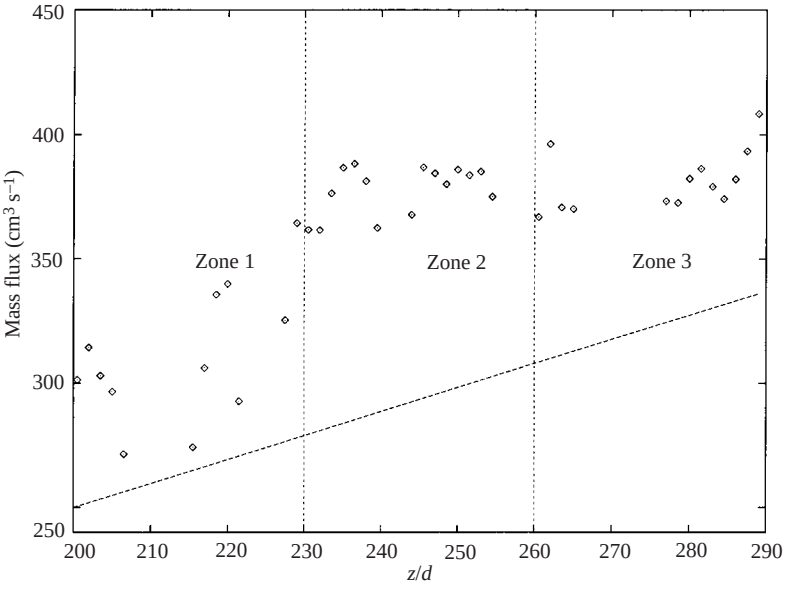

FIGURE 14. Variation of mass flux for ◇, a heated jet. ---, normal jet ($Re = 2400$, $G = 4.3$). Note that the mass flux in zones 2 and 3 is an under estimate of the true mass flux (see the accompanying text).

In summary, figures 4 and 5 provide evidence for disruption of eddies through visualization using a tracer, and figure 13(*b*) corroborates the same result through velocity measurements. Finally, an initial bulge followed by a reduction in the jet width and mass flux (shown below) is consistent with the presence of vortices in zone 1 and their subsequent disruption.

5.4. *Variation in mass flux*

Previous studies of volumetrically heated jets have reported contradictory observations of mass flux. For example, figure 12 of EBNP shows that the mass flux for the heated jet increases throughout the HIZ, at a rate exceeding that of an unheated jet. It is only in the post-HIZ that the entrainment of ambient fluid slightly reduces. In contrast, figure 10 of BN reveals that the mass flux and entrainment for the heated jet is substantially reduced in comparison to an unheated jet throughout the HIZ.

The mass flux μ is calculated here using $\mu = \pi b^2 U_c$, i.e. the mass flux can be determined by measuring b and U_c. (This expression for μ is exact for a Gaussian velocity profile.) This method of calculation is preferred over integrating the streamwise velocity profile because velocities at large radial locations (which lie outside our viewframe and are difficult to measure owing to their small magnitude) can contribute substantially to the mass flux. The plot for mass flux is shown in figure 14. The mass flux increases dramatically towards the beginning of the HIZ (zone 1), and subsequently in zones 2 and 3, the rate of increase of mass flux appears to decrease. However, based on the fact that the cross-stream velocities show an absence of outflow in the vicinity of the jet centreline (figure 7), the plateau in zones 2 and 3 should be interpreted with caution. In fact, inward velocities at large radial positions in zones 2 and 3 (see § 5.1) suggests that the mass flux should increase with downstream distance. The added mass flux beyond zone 1 appears to contribute primarily to a flattening of the streamwise velocity profile, and is therefore not so

clearly reflected in figure 14 which is calculated using b and U_c. (Agrawal *et al.* 2004*b* have shown that the mass flux of a flat-top Gaussian velocity profile is larger than a Gaussian profile jet for the same b and U_c, with the discrepancy becoming larger with increase in flatness.) Our mass flux plot shares some features with the measurements of EBNP in that our mass flux values always exceed that of an unheated jet within the HIZ. This result of a larger mass flux throughout the HIZ for heated jets as compared to their unheated counterparts is supported by the DNS study (see Agrawal *et al.* 2004*a* and § 6).

It is clear from figure 14 that the increase in mass flux is very dramatic in zone 1, and warrants an explanation. Let us consider two stations located just upstream and downstream of the beginning of the HIZ (at a distance z_1 and z_2 from the virtual origin of the jet such that $z_1 < z_b < z_2$), and assume a Gaussian velocity profile at both these stations (this assumption is justified at the base of the HIZ; see figure 6). Therefore, $\mu \sim b^2 U_c$, and momentum flux, $M \sim (bU_c)^2$. Therefore, we obtain

$$\begin{aligned}(\mu_2 - \mu_1)_{heated\ jet} &= (b^2U_c)_2 - (b^2U_c)_1 \\ &= (bU_c)_1[(1+\delta)b_2 - b_1] \quad \text{where } \frac{(bU_c)_2}{(bU_c)_1} = 1+\delta \\ &= c(bU_c)_1\left[1+\delta\tfrac{z_2}{z_2-z_1}\right](z_2 - z_1),\end{aligned}$$

assuming a constant velocity spread rate ($\mathrm{d}b/\mathrm{d}z = c$) between the two stations. (Although it is obvious that c should not be a constant, our assumption of constant c serves to simplify the analysis. It is apparent from figure 9 that heat injection causes c to increase at the base of the HIZ, therefore, the difference in mass flux between the heated and the unheated jet will be even greater. In other words, our use of a constant c provides a lower bound on the change in mass flux that should occur just because of a change in momentum flux. The experimental observation of a larger c, in fact, reinforces our argument.) Repeating the above exercise for a normal jet, we obtain

$$(\mu_2 - \mu_1)_{unheated\ jet} = c(bU_c)_1(z_2 - z_1).$$

Clearly $(\mu_2 - \mu_1)_{heated\ jet} > (\mu_2 - \mu_1)_{unheated\ jet}$ because $\delta > 0$ (for a heated jet, the addition of buoyancy will increase the local momentum). This implies that a step increase in momentum flux is followed by a step increase in mass flux as well.

A larger than normal increase in mass flux results in a large dilution. The large amount of mixing of virtually stagnant ambient fluid with the jet fluid is associated with a larger than normal decay of the centreline velocity (i.e. larger than normal deceleration). It further results in a bulge in the velocity width (see figure 9) and scalar widths (see figure 6 of BN) in zone 1. The data of VBN for a heated plume also provide evidence for this.

Extending the analysis to a third point further into the HIZ, we obtain

$$(\mu_3 - \mu_2)_{heated\ jet} = c_2(bU_c)_2\left[1+\delta_2\frac{z_3}{z_3 - z_2}\right](z_3 - z_2).$$

It is clear that $\delta_2 < \delta$, i.e. the incremental effect of heat reduces with the axial distance (the same amount of heat addition causes smaller relative increase in temperature in a warmer fluid). In other words, the relative change in momentum flux with heat addition decreases with increase in momentum. Our DNS confirms that the rate of increase in buoyancy flux is maximum at the base of the HIZ (Agrawal *et al.* 2004*a*). Further, using the observation that the increment in spread rate decreases in the latter

part of the HIZ (figure 9), it can be argued that

$$(\mu_3 - \mu_2)_{heated\ jet} < (\mu_2 - \mu_1)_{unheated\ jet}$$

i.e. the increment in mass flux will reduce with the axial distance in the latter part of the HIZ as seen in figure 14.

6. Comparison with simulations

Direct numerical simulations of the volumetrically heated jet were conducted using a suitably modified version of the turbulent jet code of Boersma *et al.* (1998) and Lubbers, Brethouwer & Boersma (2001) (see Agrawal *et al.* 2004*a* for computational details). Briefly, mass and energy conservation, and momentum and scalar transport equations were solved on a spherical grid. A traction free boundary condition was used at the lateral edge which allows physical entrainment into the computational domain. The heating rate for the simulations ($Ri = 1.2$) was of the same order as for the experiments ($Ri = 0.3$). However, computational constraints restricted the Schimdt and Prandtl numbers to unity, which is different from the experimental values of 40 and 6, respectively. The mismatch in parameters between the experiments and simulations should be kept in mind while comparing the results. The system solved here involved a three-way coupling between momentum, temperature and scalar concentration in a bid to replicate the experimental system wherein the local acid concentration determines the local heat release.

The acceleration of the jet due to heat addition, and the change in velocity profiles were clearly evident in the simulations. Further, the velocity width was larger than the scalar width in the HIZ. These results for $Ri = 1.2$ are similar to those presented in detail for $Ri = 12$ by Agrawal *et al.* (2004*a*). It is not our intention to provide a comprehensive analysis of the DNS database here; rather, we concentrate on r.m.s. and mass flux evolution to resolve disagreements with previous findings, as discussed in § 5.2 and 5.4.

The contour plot for normalized r.m.s. of the streamwise velocity obtained after time and azimuthal averaging is shown in figure 15. The behaviour for a normal jet is recovered in the pre-HIZ, as expected, with a maximum value of around 0.2 at the centreline (see also Boersma *et al.* 1998; Agrawal *et al.* 2004*a*). It is obvious from the plot that the r.m.s. is significantly larger than a normal jet for a substantial part of the HIZ and in the post-HIZ. (A lack of statistical convergence can be detected in the immediate neighbourhood surrounding the centreline because azimuthal averaging does not contribute at the centreline.) Although differences exist between experiment and simulation in the details of the axial variation, either due to differences in flow parameters or inadequate resolution at the base of the HIZ in the measurements, both datasets suggest comparable maximum r.m.s. values, and clearly lead to the conclusion that the normalized r.m.s. increases with heat addition. Furthermore, DNS corroborates an off-axis peak near the top of the HIZ, as seen in figure 10.

Figure 16 depicts mass, momentum and buoyancy flux for the volumetrically heated jet as obtained from DNS. The mass flux increases linearly in the pre-HIZ at a rate that closely matches published data. DNS indicates a larger mass flux with heating in agreement with our experimental observations. Further, the rate of entrainment also increases with heating as is apparent from the much larger slope within the HIZ. It was also verified that the entrainment coefficient is indeed larger for the volumetrically heated jet. The momentum flux remains close to unity in the pre-HIZ

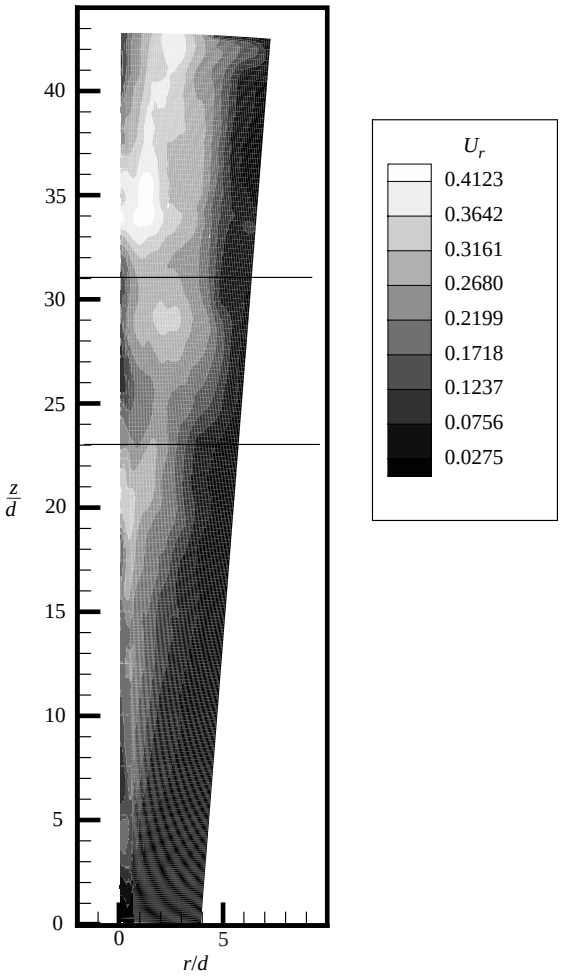

FIGURE 15. Contour plot for normalized streamwise velocity r.m.s. obtained from DNS at $Re = 1000$, $Ri = 1.2$, $Sc = Pr = 1$. The horizontal lines indicate the location of the HIZ.

as expected for an ordinary jet, and rapidly increases owing to the addition of heat in the HIZ. The added buoyancy causes the momentum flux to continuously increase in the post-HIZ as well. Finally, the buoyancy flux is zero in the pre-HIZ, increases steadily to a maximum at the end of the HIZ, and subsequently retains this value in the post-HIZ. The buoyancy flux thus accurately reflects the addition of heat within the HIZ, and the lack thereof before and after the HIZ. The maximum value attained by the buoyancy flux can be verified by energy balance. This check was performed as described in Agrawal *et al.* (2004*a*) with good agreement between the expected and simulated values.

7. Discussion

We have shown in section 5.1 that heat addition can cause the jet to decelerate upon entering the HIZ. At what point in the HIZ, then, will the jet begin to accelerate, and why? The rate of temperature rise is inversely proportional to the local streamwise

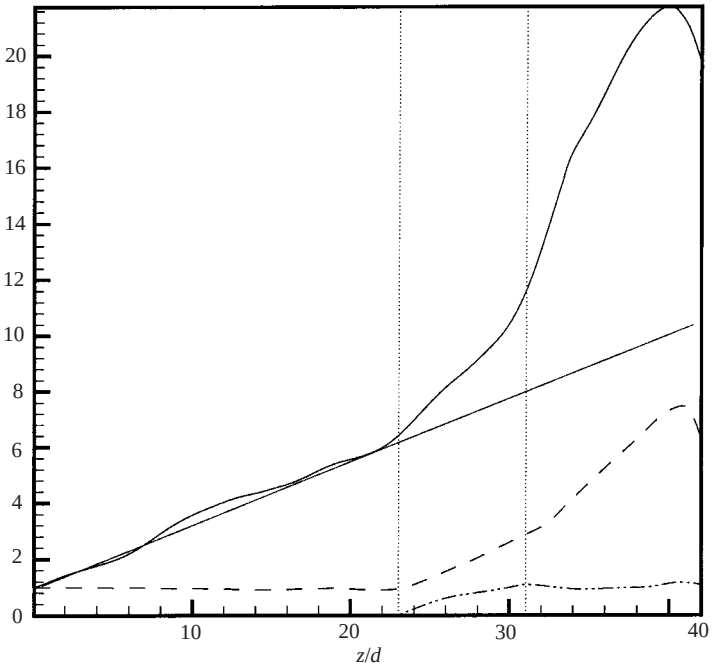

FIGURE 16. —, Mass, – – –, momentum and – · –, buoyancy fluxes from DNS at $Re = 1000$, $Ri = 1.2$, $Sc = Pr = 1$. The mass flux for the unheated jet (straight solid line) is also shown for comparison. The vertical lines indicate location of the HIZ.

velocity; a slower velocity implies a larger residence time in the HIZ, and therefore a larger temperature rise. The jet fluid entering the HIZ begins to gain buoyancy more rapidly owing to its initial deceleration, and subsequently accelerates.

The strong action of heat downstream of the point of minimum velocity results in a change of the streamwise velocity profile, i.e. the onset of zone 2. Heat injection causes the velocities to become more uniform: the velocity of the faster moving fluid near the jet centreline is increased to a smaller extent; however, the velocity of the slower moving fluid away from the jet centreline is affected more strongly. The net effect of heat on the Gaussian streamwise velocity profile is to change it to a flat-top Gaussian.

7.1. *Reasons for change in the spread rate*

Both present (figures 4, 9) and previous studies have indicated that lateral spreading of the jet is arrested in zones 2 and 3 with heat addition. This interesting observation warrants some explanation; we examine this issue using arguments by Tso & Hussain (1989). First, for a normal jet there is a flux of streamwise momentum in the radial direction, and this momentum flux term is primarily responsible for the lateral spreading of the jet (Tso & Hussain 1989). Addition of buoyancy directly increases the streamwise component of momentum flux; however, to first order, the added buoyancy does not affect the flux of streamwise momentum in the radial direction. The implication of this is that the jet travels a larger distance downstream for the same amount of lateral growth. This is partly responsible for the eventual reduction of both scalar and velocity spread rates of the heated jet. Secondly, a transverse movement of large eddies is responsible for the lateral spread of a normal jet (Tso &

Hussain 1989). We have already shown that large eddies are disrupted by heat addition in zones 2 and 3. The subsequent disruption of large eddies inhibits this mechanism of lateral growth for the jet. It is apparent that these arguments should apply to volumetrically heated plumes as well. Indeed a reduction in plume width has been reported by Venkatakrishnan *et al.* (1998) and VBN.

Figures 4 and 9 have shown a contrasting behaviour for the scalar and velocity widths of the heated jet in zones 2 and 3. While the scalar width in the latter part of the HIZ is smaller, the velocity width is larger for the heated jet as compared to its unheated counterpart. This anomalous behaviour may be related to an increased mass flux for the heated jet (P. Hug 2001, personal communication). As the heated jet begins to accelerate owing to the added buoyancy, continuity dictates that a larger amount of ambient fluid is drawn inwards to the centreline, i.e. fresh ambient fluid can be inducted by the jet owing to its acceleration. In this manner, the scalar width can actually reduce, despite a concomitant increase in velocity width.

7.2. *Coupling between concentration, velocity and temperature*

A three-way coupling exists between scalar concentration, temperature and velocity in a volumetrically heated jet. The local electrical conductivity in the jet is proportional to the local scalar concentration. Consequently, concentration affects the local temperature rise through the source term in the energy equation. The temperature field in turn is coupled to the streamwise momentum equation through the buoyancy term. Finally, the resulting velocity field affects the advection of the scalar and temperature fields. The momentum, energy and scalar equations describing this three-way interplay are provided in Agrawal *et al.* (2004*a*). The interaction between concentration, temperature and velocity results in a complicated and interesting flow field. Although this coupling is implicit in various arguments presented in the paper, we now elucidate this three-way interaction through specific observations.

We have alluded in § 5.1 (see Agrawal *et al.* 2004*b* for details) to how the combined effects of velocity and concentration fields can lead to the observed double-peaked Gaussian temperature profile. The temperature profile can be regarded as a perturbation that acts on, and eventually modifies, the velocity field. Assuming that the temperature perturbation leads to a correlated velocity perturbation, it can be shown that the superposition of a double-peaked perturbation on a Gaussian velocity profile can, in fact, reproduce a flat-top Gaussian profile for the streamwise velocity. This model fits our experimental observations: the double-peaked Gaussian profile for temperature in zone 2 is followed by a flat-top Gaussian velocity profile in zone 3. The modified velocity profile in zone 3 can, in turn, affect the temperature profile there. Evidence of a flat-top temperature profile in zone 3 can be found in Agrawal *et al.* (2004*b*).

As explained in § 7.1, the temperature field leads to a reduction in the scalar width and a plateauing of the velocity width. This behaviour again highlights the importance of the interplay between the three fields.

7.3. *Mechanisms of entrainment in a heated jet*

A primary conclusion of previous studies of volumetrically heated jets was that existing theories are unable to explain the reduction in entrainment of the jet with heat addition (see BN for a detailed discussion). They proposed that the disruption of large engulfing eddies brought about by a radial temperature gradient is responsible for the reduced entrainment in the heated jet. However, this observation is not corroborated by the plume experiments of VBN because even when the large eddies

were reportedly disrupted by heat addition, a concomitant reduction in mass flux did not occur.

As discussed in § 5.4, the mass flux of a volumetrically heated jet does not reduce, but rather shows a complicated trend. This suggests that the entrainment mechanism for heated jets is different in the three zones. The behaviour is examined in light of the existing entrainment theories.

7.3.1. *Entrainment in zone* 1

Hunt (1993) argued that a positive body force on a jet will produce a larger than normal mass flux, and the breaking up of a jet into smaller eddies will reduce the mass flux. Zone 1 shows the continued presence of large eddies (figures 4, 13*b*); further, the added buoyancy results in a positive body force. Therefore, an increased mass flux is expected in zone 1 owing to the reinforcement of both influences.

Lumley (1971) has argued that an entrainment wind causes a lateral compression of the eddies for a jet, resulting in a smaller tendency to overturn for these eddies. However, the lateral compression is offset in a plume by a vertical compression due to a positive temperature gradient near the plume-edge (the vertical temperature gradient in a plume is negative for $r/b < 0.92$ and becomes positive for larger r/b (Lumley 1971)) resulting in a larger overturning for plumes compared to jets. We now provide evidence of lateral compression of eddies in unheated jets and more circular eddies in volumetrically heated jets from LSE computations. Referring back to figure 13(*a*), the vortices centred at (12, 13), (52, 33) and (9, 53) for the unheated jet appear to be laterally compressed owing to the entrainment wind. In contrast, a heated jet experiences a positive temperature gradient and the single vortex centred at (10, 11) in figure 13(*b*) for the heated jet appears to be quite circular, and leads to higher entrainment in zone 1.

The arguments of both Hunt (1993) and Lumley (1971) are therefore consistent with a substantially larger entrainment in zone 1 (figure 14) compared to unheated jets. It should be noted that the suppressive effects of stable stratification on large eddies are not yet felt in zone 1; presumably there is a time lag associated with this effect which delays its appearance until zone 2 and beyond. Therefore, large eddies which form normally in the pre-HIZ will enter the HIZ from below and, in fact, lead to added entrainment in zone 1 as suggested by Lumley. Downstream from zone 1, stable stratification is associated with the suppression of large eddies and Lumley's argument is less relevant beyond zone 1.

7.3.2. *Entrainment in zone* 2

The argument of Hunt (1993) can be applied to zone 2 (and zone 3) as well. As the jet enters zone 2, the large eddies are disrupted and only smaller ones survive (figure 4) leading to a reduction in entrainment for zone 2 compared to zone 1. The two mechanisms identified by Hunt, in fact, appear to compete in zone 2, and the latter mechanism (due to the break up of large eddies) apparently dominates.

A viscous process of entrainment, although not important for an unstratified free shear flow, may become important for understanding mixing across interfaces in the presence of large stabilizing buoyancy forces (Turner 1986). For example, Maxworthy (1972) has suggested that vorticity diffuses across the jet boundaries into the irrotational fluid. The affected irrotational fluid can no longer move along the surface of the corrugations, and is entrained behind these corrugations. Similarly, Mathew & Basu (2002) and Bisset, Hunt & Rogers (2002) from an analysis of their

DNS data have proposed that nibbling may contribute substantially to entrainment in turbulent jets. Now Basu & Narasimha (1999) have already shown that heat injection produces a large amount of small-scale vorticity in the heated jet. It is plausible that the generation of additional vorticity leads to an increased diffusion of the turbulent interface and nibbling resulting in entrainment of the irrotational ambient fluid into the main body of the heated jet for zone 2 (and zone 3). A detailed substantiation of these theories for heated jets is beyond the scope of this work.

7.3.3. *Entrainment in zone* 3

Besides the two possible mechanisms of entrainment for zone 2 identified above, the jet experiences an acceleration in zone 3 (figure 8). This additional effect of jet acceleration can draw the ambient fluid towards its centreline. Note that this fluid is drawn inwards without the action of the large engulfing eddies which have already been suppressed. A further example of strong acceleration leading to an increased mass flux for heated jets is provided by the DNS computations of Agrawal *et al.* (2004*a*).

In summary, Hunt's (1993) arguments apply throughout the HIZ. The change in shape of the eddies in zone 1 is consistent with Lumley's (1971) hypothesis. Entrainment continues beyond zone 1 as suggested by the mechanisms of Maxworthy (1972) and Mathew & Basu (2002), and due to the acceleration effect. However, the added mass flux in zones 2 and 3 may not be clearly reflected in figure 14 because of the reasons presented in § 5.4.

It is relevant to note that a strong reduction in spread rate and entrainment has been observed in mixing layers with heat release (Hermanson & Dimotakis 1989). Dilatation effects were identified as the primary cause for this reduction. Dilatation effects in the current experiments are negligible (about three orders of magnitude smaller than in the case of Hermanson & Dimotakis 1989). For the present flow, baroclinic generation of vorticity should primarily govern entrainment; in fact, baroclinic generation of vorticity should enhance entrainment (P. E. Dimotakis 2002, personal communication). As stated above, the nibbling effect due to the baroclinic generation of small-scale vorticity observed by Basu & Narasimha (1999) provides some evidence of this.

8. Conclusions

Off-source volumetric heat was added to an axisymmetric turbulent jet in a manner developed by Bhat *et al.* (1989) to simulate the latent heat release effect in cumulus clouds. The use of whole-field velocity and temperature measurements have revealed the evolution of the volumetrically heated jet within the HIZ. We are able to demarcate three subzones with different properties within the HIZ based primarily on the nature of the cross-stream velocity profile. A deceleration in the centreline velocity, a bulge in the velocity width and an increase in the normalized streamwise r.m.s. characterize the entry zone of the HIZ (zone 1). An interesting double-peaked Gaussian temperature profile and disruption of large eddies are seen in the middle zone (zone 2) along with substantially larger r.m.s. values compared to normal jets. A flat-top Gaussian streamwise velocity profile and an inward cross-stream velocity profile are observed in the exit zone of the HIZ (zone 3). These results are summarized in figure 17.

Explanations are provided for these results. The flattening of the streamwise velocity profile is consistent with the increased streamwise momentum flux due to heat addition. Because the momentum flux is larger for heated jets as compared to their

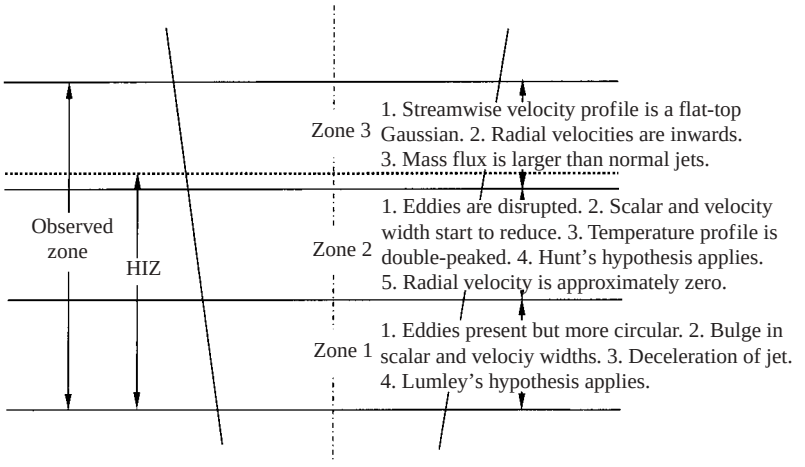

FIGURE 17. Summary of observations of the three zones in a volumetrically heated jet.

unheated counterparts, the flattening of the streamwise velocity profile occurs to accommodate a larger streamwise momentum flux.

The initial increase in centreline deceleration corresponds to a wider than normal jet. The subsequent increase in the centreline velocity is due to the addition of buoyancy, and is responsible for an inflow for all radial locations in the viewframe. Heat injection causes an increase in the normalized fluctuation of the streamwise velocity indicating that relaminarization of the jet does not occur. Further, heat addition causes the r.m.s. velocity profiles to become nearly uniform near the jet centreline.

The disruption of large eddies results in a reduction of the scalar width, and eventually, a flattening of the velocity width as well. Additionally, an increase in the streamwise component of momentum without a corresponding change in the flux of streamwise momentum in the radial direction has been recognized as the primary mechanism responsible for the observed reduction in the lateral growth rate (scalar width) of a heated jet.

The mass flux increases rapidly at the beginning of the HIZ, and is always larger than its unheated counterpart. A larger mass flux for the heated jet is corroborated with the DNS computations, which further suggest that the entrainment rate can also increase with heat addition. We argue mathematically that a step change in momentum flux correlates with a step change in mass flux, resulting in an initial bulge in the velocity width towards the beginning of the HIZ. The arguments of Hunt (1993) and Lumley (1971) are evaluated to explain an increased entrainment at the beginning of the HIZ.

It is relevant to compare our findings with those of previous workers. We found disruption of large eddies and reduction of scalar width in agreement with EBNP and BN. However, our linear stochastic estimates showed that this disruption occurs only in the latter part of the HIZ. We also provide a more convincing measurement of the velocity width. A larger relative deceleration was observed at the beginning of the HIZ in agreement with VBN. Similarly, our r.m.s. measurements bear some resemblence with those of VBN, but are not in general agreement with those of EBNP and BN. Our experimental mass flux plot is similar to that of EBNP, but differs from BN. Some of our experimental results agree better with the heated plume results of VBN than with the heated jet results of both EBNP and BN. A probable reason is

the consistent presence of a 'bulge' at the base of the HIZ in VBN and our data, that significantly affects the properties further downstream in the HIZ. Probable reasons for the disagreement have been presented in the paper, along with several new results and their explanations.

It is also relevant to connect the results from the heated jet experiments to cloud entrainment. We have observed that the scalar width reduces upon volumetric heat addition. This result is consistent with photographs of cumulus clouds which are generally characterized by vertical boundaries. Secondly, we have observed that the velocity width of the heated jet increases initially upon entering the HIZ and then reaches a constant value. A direct comparison of this feature with clouds is difficult owing to a paucity of such data in the cloud literature. Thirdly, the observation of Bretherton & Smolarkiewicz (1989) that an increase of vertical acceleration with height within the cloud induces inflow from the environment, and may result in enhanced entrainment, is consistent with our observation of the acceleration of the jet leading to an increase in entrainment.

The authors thank Dr K. R. Sreenivas of the Jawaharlal Nehru Center of Advanced Scientific Research, India and Professor Pablo Huq of the University of Delaware, USA for several useful discussions which were critical for the development of this work. We are grateful to Dr B. J. Boersma of Delft University of Technology, the Netherlands for making the DNS code available to us. A.A. is grateful to Professors P. E. Dimotakis of Caltech, USA and J.C.R. Hunt of Delft Institute of Technology, the Netherlands for sharing their insights. We also thank the anonymous reviewers for their comments and suggestions. This work was supported by National Science Foundation, under grant NSF-ATM-0095122.

REFERENCES

Adrian, R. J. 1994 Stochastic estimation of conditional structure: a review. *Appl. Sci. Res.* **53**, 291.

Agrawal, A. 2002 Effect of off-source volumetric heat addition on entrainment in a turbulent jet with application to cumulus clouds. PhD dissertation, University of Delaware.

Agrawal, A., Boersma, B. J. & Prasad, A. K. 2004*a* Direct numerical simulation of a turbulent axisymmetric jet with buoyancy-induced acceleration. *Flow Turb. Combust.* (to appear).

Agrawal, A. & Prasad, A. K. 2002*a* Properties of vortices in a self-similar turbulent jet. *Exps. Fluids* **33**, 565.

Agrawal, A. & Prasad, A. K. 2002*b* Organizational modes of large-scale vortices in an axisymmetric turbulent jet. *Flow Turb. Comb.* **68**, 359.

Agrawal, A., Sreenivas, K. R. & Prasad, A. K. 2004*b* Velocity and temperature measurements in an axisymmetric turbulent jet with cloud-like off-source heating. *Intl J. Heat Mass Transfer* **47**, 1433.

Basu, A. J. & Narasimha, R. 1999 Direct numerical simulation of turbulent flows with cloud-like off-source heating. *J. Fluid Mech.* **385**, 199.

Bhat, G. S. & Narasimha, R. 1996 A volumetrically heated jet: large eddy structure and entrainment characteristics. *J. Fluid Mech.* **325**, 303 (referred to herein as BN).

Bhat, G. S., Narasimha, R. & Arakeri, V. H. 1989 A new method of producing local enhancement of buoyancy in liquid flows. *Exps. Fluids* **7**, 99.

Bisset, D. K., Hunt, J. C. R. & Rogers, M. M. 2002 The turbulent/non-turbulent interface bounding a far wake. *J. Fluid Mech.* **451**, 383.

Boersma, B. J., Brethouwer, G. & Nieuwstadt, F. T. M. 1998 A numerical investigation on the effect of the inflow conditions on the self-similar region of a round jet. *Phys. Fluids* **10**, 899.

Bretherton, C. & Smolarkiewicz, P. 1989 Gravity waves, compensating subsidence and detrainment around cumulus clouds. *J. Atmos. Sci.* **46**, 740.

Elavarasan, R., Bhat, G. S., Narasimha, R. & Prabhu, A. 1995 An experimental study of a jet with local buoyancy enhancement. *Fluid Dyn. Res.* **16**, 189 (referred to herein as EBNP).

Emanuel, K. A. 1994 *Atmospheric Convection.* Oxford University Press.

Gieseke, T. J. & Guezennec, Y. G. 1994 Stochastic estimation of multipoint conditional averages and their spatio-temporal evolution. *Appl. Sci. Res.* **53**, 305.

Govindarajan, R. 2002 Universal behavior of entrainment due to coherent structures in turbulent shear flow. *Phys. Rev. Lett.* **88**, 134503.

Hermanson, J. C. & Dimotakis, P. E. 1989 Effect of heat release in a turbulent, reacting shear layer. *J. Fluid Mech.* **199**, 333.

Heymsfield, A. J., Johnson, P. N. & Dye, J. E. 1978 Observations of moist adiabatic ascent in northeast colorado cumulus congestus clouds. *J. Atmos. Sci.* **35**, 1689.

Hunt, J. C. R. 1993 Atmospheric jets and plumes. In *Recent Res. Adv. Fluid Mech. Turb. Jets Plumes*, **309**.

Hussein, H. J., Capp, S. P. & George, W. K. 1994 Velocity measurements in a high-Reynolds-number, momentum-conserving, axisymmetric turbulent jet. *J. Fluid Mech.* **258**, 31.

Lubbers, C. L., Brethouwer, G. & Boersma, B. J. 2001 Simulation of the mixing of a passive scalar in a round turbulent jet. *Fluid Dyn. Res.* **28**, 189.

Lumley, J. L. 1971 Explanation of thermal plume growth rates. *Phys. Fluids* **14**, 2537.

Mathew, J. & Basu, A. J. 2002 Some characteristics of entrainment at a cylindrical turbulence boundary. *Phys. Fluids* **14**, 2065.

Maxworthy, T. 1972 The structure and stability of vortex rings. *J. Fluid Mech.* **51**, 15.

Morton, B. R. 1957 Buoyant plumes in a moist atmosphere. *J. Fluid Mech.* **2**, 127.

Narasimha, R., Saxena, V. & Kailas, S. V. 2002 Coherent structures in plumes with and without off-source heating using wavelet analysis of flow imagery. *Exps. Fluids* **33**, 196.

Paluch, I. R. 1979 The entrainment mechanism in Colorado cumuli. *J. Atmos. Sci.* **36**, 2467.

Prasad, A. K. & Gonuguntla, P. V. 1996 Turbulence measurements in non-penetrative thermal convection. *Phys. Fluids* **8**, 2460.

Scorer, R. 1972 *Clouds of the World – A Complete Color Encyclopedia.* Lothian.

Siddhartha, S. S., Narasimha, R., Basu, A. J. & Kailas, S. V. 2000 Coherent structures in numerically simulated jets with and without off-source heating. *Fluid Dyn. Res.* **26**, 105.

Squires, P. & Turner, J. S. 1962 An entraining model for cumulonimbus updrafts. *Tellus* **14**, 1067.

Sreenivas, K. R. & Prasad, A. K. 2000 Vortex-dynamics model for entrainment in jets and plumes. *Phys. Fluids* **12**, 2101.

Tso, J. & Hussain, F. 1989 Organized motions in a fully developed turbulent axisymmetric jet. *J. Fluid Mech.* **203**, 425.

Turner, J. S. 1986 Turbulent entrainment: the development of the entrainment assumption, and its application to geophysical flows. *J. Fluid Mech.* **173**, 431.

Venkatakrishnan, L., Bhat, G. S. & Narasimha, R. 1999 Experiments on a plume with off-source heating: implications for cloud fluid dynamics. *J. Geophy. Res.* **104**, 14271 (referred to herein as VBN).

Venkatakrishnan, L., Bhat, G. S., Prabhu, A. & Narasimha, R. 1998 Visualization studies of cloud-like flows. *Curr. Sci.* **74**, 597.

Warner, J. 1970 On steady-state one-dimensional models of cumulus convections. *J. Atmos. Sci.* **27**, 1035.